Sensors and Materials, Vol. 38, No. 7 (2026) 4097–4110
MYU Tokyo

S & M 4552

Automated Cylindrical Electromagnetic Shielding Enclosure with Ferrite-based Microwave-absorbing O-rings

Ke-Hua Chen,[1] Wei Chien,[2] Meng-Chun Li,[3]
Chao-Ming Hsu,[3*] and Cheng-Fu Yang[4,5**]

[1]College of Information Engineering, Ningde Normal University, Ningde, Fujian 352100, China
[2]Department of Electrical Engineering, Tatung University, Taipei 104327, Taiwan
[3]Department of Mechanical Engineering, National Kaohsiung University of Science and Technology, Kaohsiung 807, Taiwan
[4]Department of Chemical and Materials Engineering, National University of Kaohsiung, Kaohsiung 811, Taiwan
[5]Department of Aeronautical Engineering, Chaoyang University of Technology, Taichung 413, Taiwan

(Received January 29, 2026; accepted July 3, 2026)

Keywords: fifth-generation (5G) communication systems, IoT, electromagnetic interference (EMI), O-ring-shaped microwave-absorbing composites

The rapid deployment of fifth-generation (5G) communication systems has accelerated the growth of IoT, while simultaneously intensifying electromagnetic interference (EMI), which adversely affects sensor stability and measurement accuracy. To address this challenge, we propose an automated cylindrical electromagnetic shielding enclosure operating in the low-frequency 5G band, designed to provide an interference-free environment for sensor testing and quality control. The enclosure is fabricated from aluminum alloy and designed to meet IP68 sealing requirements, with a tapered contact interface to minimize signal leakage. To achieve high shielding effectiveness, O-ring-shaped microwave-absorbing composites were developed by mixing ferrite powders of Fe_3O_4 with epoxy resin at weight fractions of 15, 20, and 25%. In addition, the hybrid arrangements of copper sheets with one-layer, two-layer, and three-layer aluminum foils were also used to investigate the EMI suppression. EMI shielding performance under different compressive pressures was experimentally evaluated using S-parameter (S21) measurements obtained from a vector network analyzer with unidirectional antennas. Although further improvements in broadband EMI shielding performance and high-frequency applications remain desirable, the proposed design addresses practical challenges associated with signal leakage and shielding stability by integrating automated pneumatic compression, ferrite-filled microwave-absorbing O-rings, and multilayer metallic shielding structures. The results demonstrate that the proposed shielding enclosure achieves high radio-frequency signal attenuation performance and effectively suppresses EMI, providing a stable and reliable testing platform for sensor-oriented IoT devices in 5G environments. Unlike recently reported cylindrical shielding enclosures that mainly rely on metallic shielding structures, the proposed design integrates automated pneumatic compression, ferrite-filled microwave-absorbing

*Corresponding author: e-mail:jammy@nkust.edu.tw
**Corresponding author: cfyang@nuk.edu.tw
https://doi.org/10.18494/SAM6232

O-rings, and multilayer metallic shielding to simultaneously enhance shielding effectiveness, attenuation stability, and testing repeatability.

1. Introduction

The rapid expansion of the wireless communication industry has driven a considerable increase in demand for RF products, particularly with the widespread deployment of fifth-generation (5G) communication systems. While 5G has enabled high-speed data transmission, massive connectivity, and low-latency communication essential for IoT applications, it has simultaneously intensified electromagnetic interference (EMI) concerns.[1,2] In dense RF environments, the coexistence of 5G, WiFi, Bluetooth, and legacy cellular signals introduces significant electromagnetic noise that can severely degrade sensor performance.[3] For sensor-based systems, especially those designed to detect weak electrical, environmental, or physiological signals, EMI can lead to signal distortion, reduced measurement accuracy, and unstable operation.[4,5] Consequently, ensuring an interference-free environment has become a fundamental requirement in sensor development, calibration, and validation. Electromagnetic shielding enclosures therefore play a critical role in modern sensor engineering by isolating devices under test from external disturbances. Shielding systems capable of providing ultrahigh attenuation are particularly valuable, as they allow sensor performance to be evaluated on the basis of intrinsic characteristics rather than environmental artifacts.[6,7] Recent studies have demonstrated that electromagnetic shielding enclosures for 5G and IoT applications have evolved beyond conventional metallic housings by incorporating advanced absorbing materials, multilayer shielding structures, optimized enclosure geometries, and automated testing mechanisms to improve shielding effectiveness, measurement repeatability, and compatibility with high-frequency wireless systems. These developments have further expanded the application of shielding enclosures in sensor characterization, RF qualification, and intelligent manufacturing environments.[8] In this context, high-performance shielding enclosures are no longer auxiliary tools but essential infrastructure supporting reliable sensor research and industrial deployment in 5G-enabled IoT ecosystems.

Accurate RF testing is an indispensable step in the production and qualification of wireless electronic products, and it represents one of the most complex and influential stages in modern manufacturing lines. Prior to shipment, IoT devices and sensor modules must undergo comprehensive RF measurements, including antenna calibration, transmission efficiency, and signal integrity evaluation. Any reduction in test yield during this stage can significantly decrease production throughput and increase manufacturing costs. The causes of low pass rates are multifaceted, involving device design, material properties, measurement uncertainty, and environmental EMI. By employing a well-designed shielding enclosure, the effect of environmental uncertainty can be substantially reduced, enabling RF tests to be performed in a stable and reproducible electromagnetic environment. For sensor-integrated wireless modules, this controlled environment is particularly important, as RF instability can directly propagate into sensing errors and unreliable data transmission. High-attenuation shielding enclosures improve test efficiency, reduce component damage during repeated measurements, and enhance confidence in test results. From the perspective of sensor quality assurance, EMI shielding is therefore a key enabler for achieving high yield, consistent performance, and robust system reliability in large-scale IoT device production.(9)

In addition to measurement accuracy, testing efficiency and automation have become critical requirements as IoT sensor markets continue to expand. The increasing adoption of smart sensors in industrial automation, smart homes, automotive electronics, and smart cities demands high-throughput testing solutions that can be seamlessly integrated into production lines. Automated shielding enclosures provide a practical solution by enabling repeatable and standardized RF measurements with minimal human intervention. Cylindrical shielding designs are particularly suitable for automated operation, as they facilitate uniform mechanical compression, reliable sealing, and consistent antenna positioning. Automation not only reduces operator-induced variability but also shortens testing cycles, thereby accelerating time-to-market for sensor-based IoT products. For sensors operating in 5G environments, automated testing within a highly shielded enclosure ensures that both sensing and communication functions are evaluated under realistic yet interference-free conditions. This approach supports scalable manufacturing while maintaining the precision required for advanced sensing applications, such as industrial condition monitoring, intelligent transportation systems, and biomedical IoT devices.

Beyond basic RF performance evaluation, high-performance shielding enclosures are essential for advanced IoT transmission scenarios, including multi-band coexistence testing, ultra-low-latency verification, and data security assurance. Modern IoT devices often integrate multiple wireless standards such as 5G New Radio (NR), Long-Term Evolution (LTE), WiFi 6, Bluetooth 5.x, and Narrowband Internet of Things (NB-IoT) within a single platform. Interference among these bands can complicate performance assessment and lead to misleading conclusions if not properly isolated. A high-attenuation shielding enclosure allows individual frequency bands to be evaluated independently, ensuring the accurate characterization of each communication channel and its interaction with embedded sensors. Moreover, emerging 5G IoT applications emphasize ultra-reliable and low-latency communication, which is critical for time-sensitive sensing tasks in industrial automation and remote healthcare.(10,11) Shielded environments enable precise latency measurements by eliminating external signal fluctuations. In addition, shielding enclosures prevent unintended signal leakage during development and testing, thereby protecting sensitive sensor data from eavesdropping or unauthorized access. These capabilities highlight the multifunctional role of shielding systems in supporting reliable, secure, and high-performance sensor-centric IoT technologies.

Compared with conventional rectangular shielding enclosures, cylindrical structures offer inherent electromagnetic and mechanical advantages that are particularly beneficial for sensor testing. The curved geometry reduces sharp edges and corners, which are known to induce strong reflections and standing-wave effects, resulting in a more uniform electromagnetic field distribution. This is especially advantageous for testing sensor nodes equipped with omnidirectional antennas, as it enables more representative radiation and reception measurements. Despite recent progress in cylindrical electromagnetic shielding enclosures, several challenges remain, including RF signal leakage at mechanical interfaces, performance degradation under varying compressive loads, and maintaining stable EMI shielding performance over a broad frequency range. These issues are particularly important for automated sensor testing, where repeatability and testing consistency are essential. To address these challenges, in the present work, we integrate a tapered sealing interface, automated pneumatic compression, ferrite-filled microwave-absorbing O-rings, and multilayer metallic shielding structures within a cylindrical enclosure. Although further studies are required to extend the shielding effectiveness over a wider frequency range, reduce the enclosure size for compact industrial deployment, and optimize the electromagnetic design through advanced simulation and experimental validation, the proposed enclosure provides a practical solution for improving shielding stability and RF testing reliability in 5G-enabled IoT environments. Building upon these advantages, we present an automated cylindrical shielding enclosure designed for the low-frequency 5G band (1–7.5 GHz), targeting an ultrahigh attenuation. Recently developed cylindrical shielding enclosures mainly focus on improving shielding effectiveness through conductive metallic shells or structural optimization. However, they generally lack integrated absorbing components, automated compression mechanisms, and the systematic evaluation of shielding stability under different mechanical loading conditions. In contrast, the proposed design combines a tapered sealing interface, automated pneumatic compression, ferrite-filled microwave-absorbing O-rings, and multilayer metallic shielding structures into a single cylindrical enclosure.(12) This integrated design not only improves RF signal attenuation but also enhances RF signal attenuation stability and testing repeatability, thereby providing a controlled electromagnetic environment that is expected to support reliable sensor characterization and automated RF testing in future practical applications. To the best of our knowledge, this is one of the few studies that simultaneously integrate structural design, absorbing materials, and automated compression mechanisms within a cylindrical shielding enclosure for sensor-oriented RF testing applications.

In this study, the term *attenuation* refers to the reduction in transmitted RF signal power caused by the electromagnetic shielding enclosure. The RF signal attenuation is quantified from the measured S21 transmission parameter, where a larger attenuation (more negative S21 value in dB) indicates a more effective suppression of RF signal propagation through the enclosure. To enhance shielding effectiveness, O-ring-shaped microwave-absorbing composites were fabricated by mixing Fe_3O_4 ferrite powders with epoxy resin at weight fractions of 15, 20, and 25%. Fe_3O_4 ferrite powder was selected as the microwave-absorbing filler because it exhibits excellent magnetic loss characteristics, high chemical stability, relatively low cost, and good compatibility with epoxy resin.(13) Compared with many other microwave-absorbing materials, Fe_3O_4 provides an effective balance between electromagnetic absorption capability, mechanical robustness, fabrication simplicity, and economic feasibility, making it particularly suitable for fabricating microwave-absorbing O-rings for shielding applications. Although other absorbing materials such as carbon-based materials, spinel ferrites, and magnetic alloys have also been reported, Fe_3O_4 was selected in this study because of its well-established performance and ease of integration into the proposed enclosure design. In parallel, hybrid shielding structures were fabricated by combining a single copper sheet with one, two, or three layers of aluminum foil to evaluate the effect of aluminum foil stacking on EMI shielding performance. By integrating material engineering, structural optimization, and sensor-oriented testing considerations, we provide a practical and scalable shielding solution for reliable RF and sensor evaluation in 5G-enabled IoT environments. Although we focus on validating the EMI shielding performance of the enclosure itself in the present work, future studies will incorporate practical sensor modules to further verify its effectiveness for sensor characterization, automated RF testing, and quality control.

2. Equipment and Measurements

The shielding enclosure fabricated in this study has overall dimensions of 300 × 240 × 515 mm, as shown in Fig. 1(a). The enclosure was designed to satisfy the IP68 sealing requirement, indicating complete protection against dust ingress and the capability to maintain its sealing performance under prolonged water immersion. Although the present study focuses on electromagnetic shielding performance rather than waterproof testing, the IP68-compliant mechanical sealing design also helps minimize RF signal leakage at the enclosure interfaces. The main components of the proposed shielding enclosure and their functions, illustrated in Fig. 1(b), are summarized as follows.

1 Rotary pressing cylinder: applies pneumatic pressure to secure the pressing rod onto the top cover of the main enclosure; in combination with a solenoid valve, automated operation is achieved.
2 Pressing rod: connects the pressing cylinder and the top cover. A 3D-printed tip is installed inside to hold the test chip above the measurement stage.
3 Tip: gently presses and fixes the test chip on the measurement stage.
4 Top cover of the main enclosure: uses tapered mating surfaces with both the enclosure body and the pressing rod to ensure tight sealing. Grooves filled with shielding powder and pneumatically compressed O-rings are incorporated into the enclosure to provide the secondary attenuation of RF signal leakage through the shielding interface.
5 Measurement stage: acts as a platform for placing the test chip.
6 Main enclosure body: houses the test chip and is equipped with SMA connectors, filters, and a 6-pin connector for RF signal input and electrical interfacing with external control systems.
7 Filter module: includes selectable USB, RS-232, and RJ-45 interfaces.
8 Support legs: provide mechanical support for the entire enclosure.
9 Control box: contains openings for air tubes, power cables, and a display. Internal space accommodates circuit boards and solenoid valves for automation.
10 Base plate: serves as the upper cover of the control box.
11 Connecting rods: link the two support legs to enhance structural stability and load bearing.

The automation of the proposed shielding enclosure is achieved through a pneumatic rotary cylinder controlled by a solenoid valve. During operation, compressed air supplied by the pneumatic system automatically actuates the pressing mechanism to open and close the enclosure without manual intervention. The control box provides the electrical interfaces required for synchronization with external testing equipment, allowing the enclosure to be incorporated into automated RF measurement workflows. Although the present prototype does

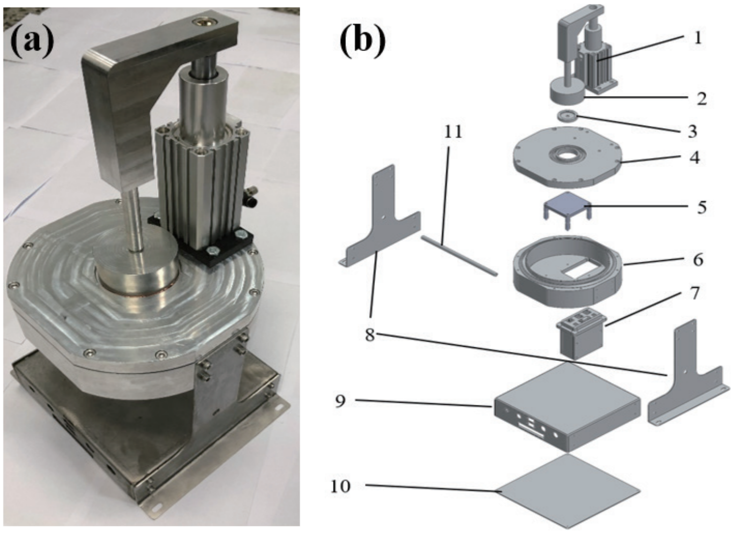

Fig. 1. (Color online) (a) Photograph of the enclosure and (b) enlarged view of the main components of the enclosure.

not incorporate dedicated sensing elements for motion control, the architecture is compatible with external sensors and programmable controllers for future intelligent automation. In future implementations, the pneumatic compression system can be further enhanced by integrating a pressure sensor within the air supply line or compression chamber to continuously monitor the applied pressure. The measured pressure can be transmitted to a programmable controller, which adjusts the solenoid valve or pressure regulator through a closed-loop feedback strategy to maintain the desired compression force. Such pressure monitoring and feedback control would improve compression consistency, compensate for pressure fluctuations, and further enhance the repeatability and reliability of automated RF measurements.

A vector network analyzer (VNA) was employed to measure the S-parameters, enabling the quantitative evaluation of the attenuation of the transmitted RF signal caused by the shielding enclosure. In this work, attenuation is defined as the reduction in RF signal transmission through the enclosure and is quantified using the measured S21 transmission parameter expressed in decibels (dB). The measured parameters included the attenuation of the bare enclosure, the enclosure equipped with O-ring absorbers containing different powder weight fractions, various configurations of aluminum foils and copper sheets with different numbers of layers, and conditions under different applied compressive pressures. The experimental setup consisted of a VNA, a VNA calibration kit, unidirectional antennas operating from 1 to 7 GHz, and a pressure regulation system, as shown in Fig. 2(a). The observation point was positioned 5 cm above the upper compression cover of the enclosure, as the interface between the compression column and the enclosure lid is the most probable location for signal leakage. Measurements were conducted at the right and front sides around the compression rod, as shown in Fig. 2(b). The observation point and the potential RF signal leakage path are explicitly illustrated in Fig. 2(b) to clarify the

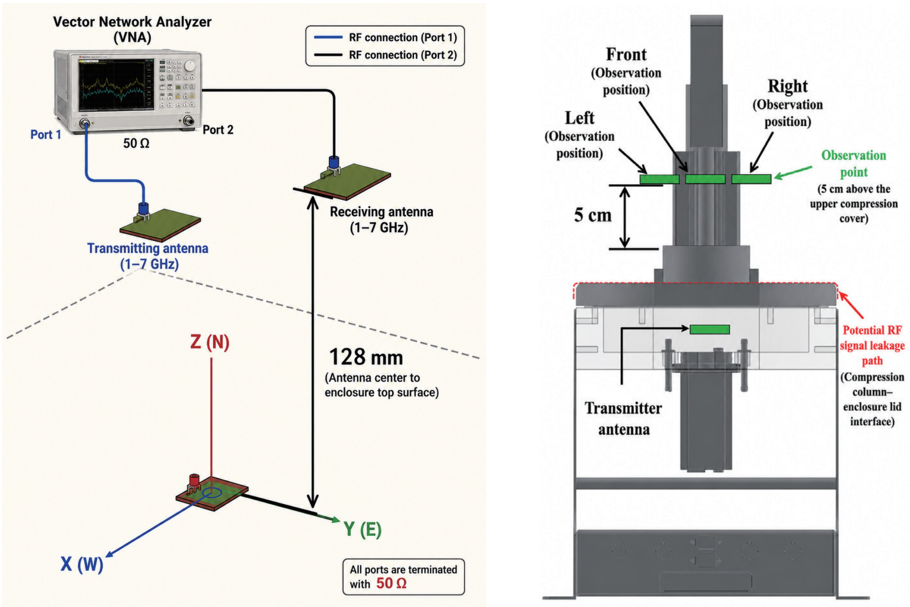

(a) (b)

Fig. 2. (Color online) Schematic illustration of the experimental measurement configuration: (a) antenna arrangement and measurement distance, and (b) observation point located 5 cm above the enclosure together with the potential RF signal leakage path.

measurement configuration. As indicated in Fig. 2(b), the observation point was located 5 cm above the upper compression cover directly above the compression column–enclosure lid interface, which was considered the most probable RF signal leakage path. The antenna separation and alignment followed the experimental configuration depicted in Fig. 2(b), with a face-to-face antenna distance of 128 mm, corresponding to 50 mm above the enclosure, and both ports terminated with a 50 Ω reference impedance.

Compressive pressure was applied using a pneumatic system. Pressurized air was delivered by a miniature pump to a pressure regulator and then transmitted to a rotary compression cylinder, which exerted force on the enclosure lid. Three pressure levels, namely, 0.2, 0.4, and 0.6 MPa, were applied to investigate the effect of mechanical loading on RF signal attenuation performance. The ferrite Fe_3O_4 powders were used to fabricate the microwave-absorbing O-rings. Each powder was mixed with epoxy resin at 15, 20, and 25 wt%. Owing to the pellet-based fabrication process, as shown in Fig. 3(a), the O-ring dimensions were designed according to standard mechanical O-ring compression guidelines. The rectangular base height was 1.16 mm, the upper semicircular height was 1.55 mm, and the designed compression ratio ranged from 9.15 to 13.3%. After compression, the total height ranged from 2.39 to 2.46 mm, and the groove depth was set to 2.4 mm. The fabricated O-rings were placed in the designed grooves for RF signal attenuation measurements, as shown in Fig. 3(b), which is the component 6 shown in Fig. 1(b).

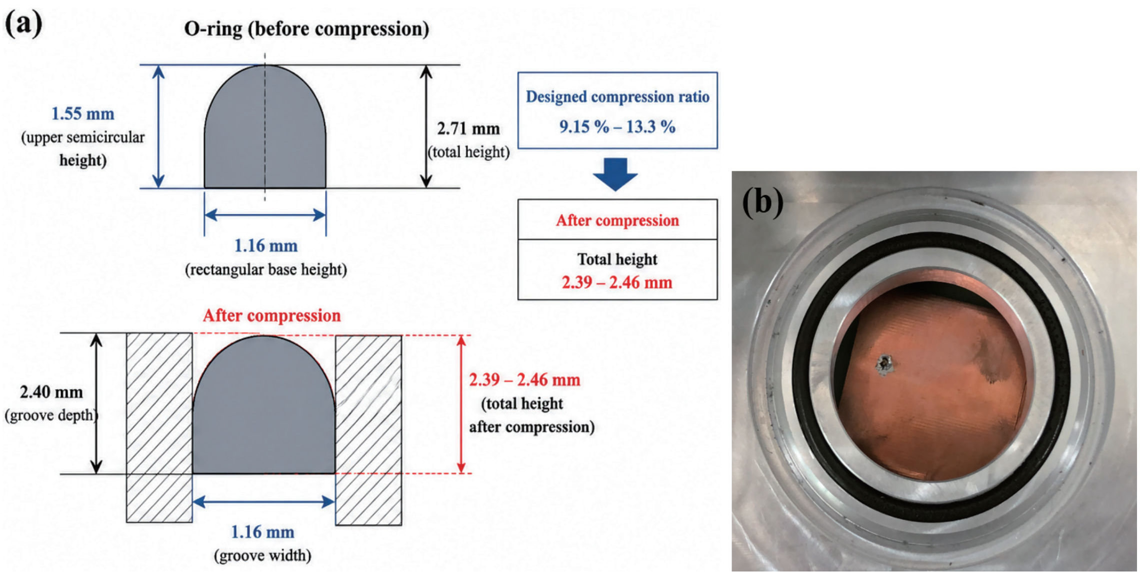

Fig. 3. (Color online) (a) Isometric view of the O-ring and (b) photograph of the O-ring placement.

3. Experimental Results and Discussion

Figure 4 presents the attenuation variations measured at the right side of the pressing rod [as illustrated in Fig. 2(b)] for Fe_3O_4-based O-rings with different weight fractions under various applied pressures at selected frequencies. Each data point represents the average of more than five repeated measurements, and the corresponding measurement errors are indicated in the figure. The label "None" denotes the reference condition in which the O-ring contains no Fe_3O_4 powder. Representative frequencies within the 1–7.5 GHz range were selected to evaluate frequency-dependent attenuation behavior. At 1 GHz [Fig. 4(a)], most configurations exhibit relatively stable attenuation regardless of pressure and Fe_3O_4 content. However, the 25 wt% sample under zero pressure and the 20 wt% sample at 0.4 MPa show comparatively lower attenuation, approximately −30 dB, indicating insufficient mechanical compression or suboptimal material distribution under these conditions. Aside from these cases, the attenuation variation at 1 GHz remains limited.

In contrast, the frequency-dependent results shown in Figs. 4(b)–4(f) reveal a pronounced effect of Fe_3O_4 loading on RF signal attenuation stability. When no Fe_3O_4 powder is incorporated, the attenuation exhibits large fluctuations across different pressures and frequencies, suggesting poor and unstable EMI suppression. Notably, the O-ring containing 25 wt% Fe_3O_4 under an applied pressure of 0.4 MPa achieves the maximum attenuation of approximately −58 dB, demonstrating enhanced and consistent EMI shielding performance. Overall, these results indicate that incorporating appropriate amounts of Fe_3O_4 powder into the O-ring significantly improves RF signal attenuation stability over a wide frequency range. Such stable EMI suppression is particularly beneficial for sensor-oriented measurement environments, where consistent attenuation is essential for ensuring reliable signal acquisition and repeatable testing under varying mechanical conditions.

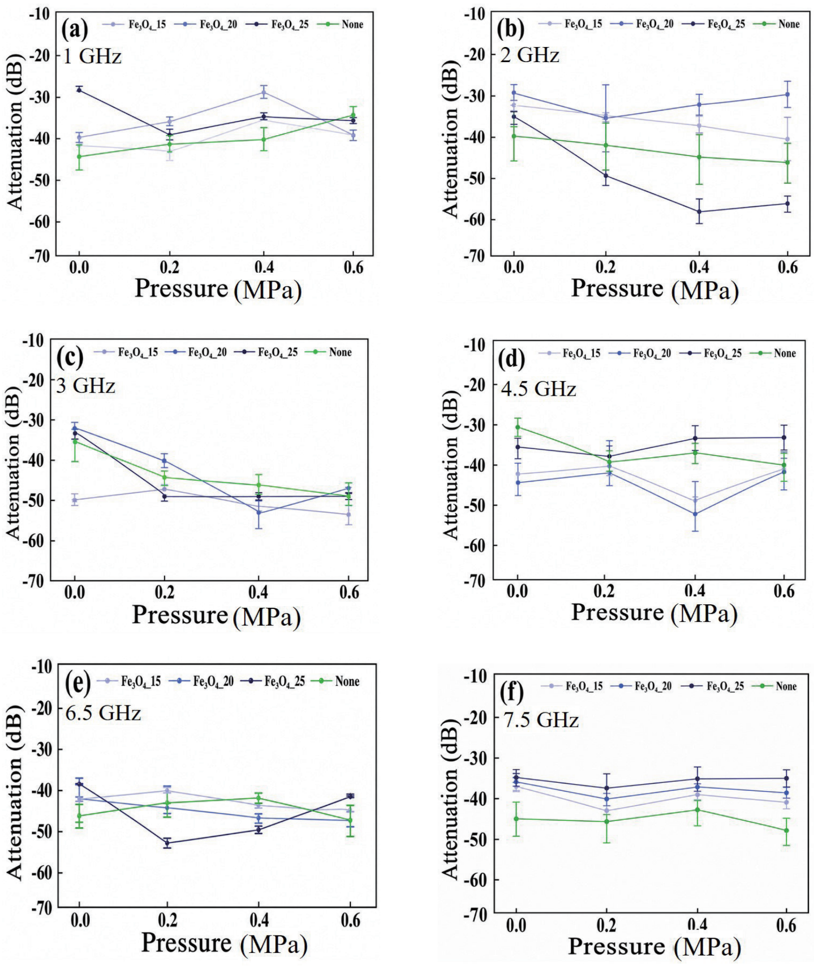

Fig. 4. (Color online) Attenuation variations measured at the right side of the pressing rod for Fe_3O_4 powder with different weight fractions under different applied pressures at various frequencies: (a) 1, (b) 2, (c) 3, (d) 4.5, (e) 6.5, and (f) 7.5 GHz.

Figure 5 presents the attenuation variations measured at the front side of the pressing rod [as illustrated in Fig. 2(b)] for Fe_3O_4-based O-rings with different weight fractions under various applied pressures at selected frequencies. As shown in Fig. 5, a notable enhancement in attenuation is observed only at 4 GHz, where the O-rings containing 25 wt% Fe_3O_4 under applied pressures of 0.4 and 0.6 MPa exhibit a higher attenuation than the O-ring without Fe_3O_4 powder. Under most other frequency and pressure conditions, the increase in absolute attenuation remains limited. Despite the modest improvement in peak attenuation, Fig. 5 clearly demonstrates that O-rings incorporating Fe_3O_4 powder at different weight fractions yield more stable attenuation results than the O-ring without Fe_3O_4. This stability is reflected by the smaller measurement error bars across repeated tests. A similar trend was observed in the results measured at the right side of the pressing rod (Fig. 4), where Fe_3O_4-filled O-rings exhibited a reduced fluctuation in attenuation under varying pressures and frequencies. The improved stability can be attributed to the presence of magnetic loss mechanisms introduced by Fe_3O_4

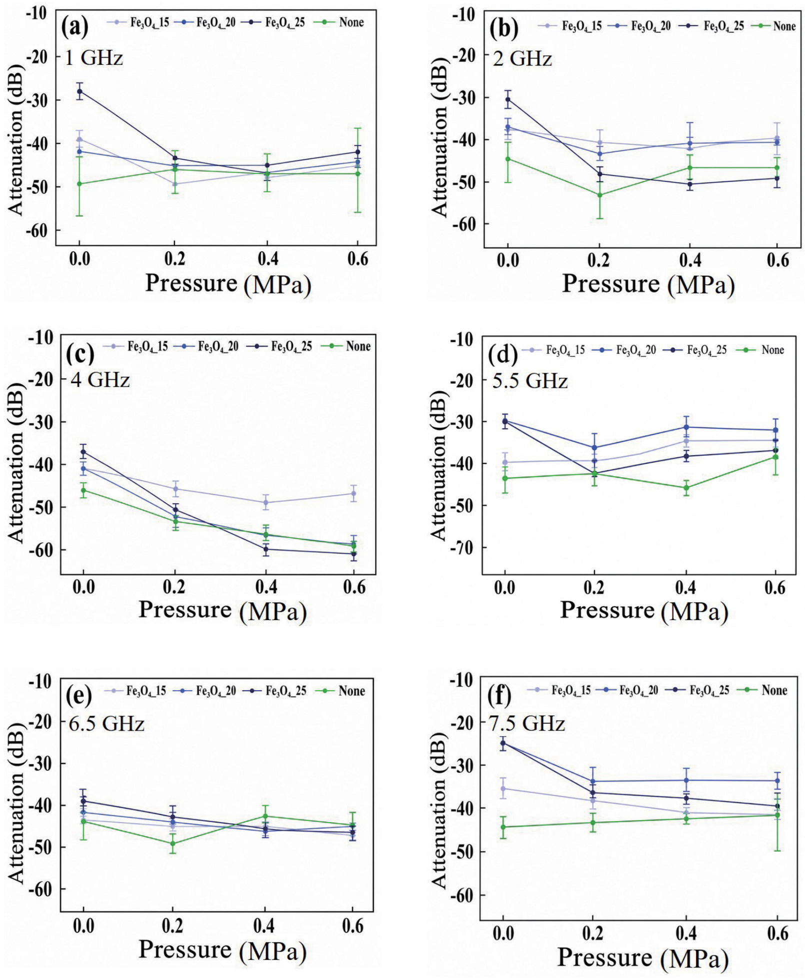

Fig. 5. (Color online) Attenuation variations measured at the front side of the pressing rod for Fe_3O_4 powder with different weight fractions under different applied pressures at various frequencies: (a) 1, (b) 2, (c) 4, (d) 5.5, (e) 6.5, and (f) 7.5 GHz.

particles, which provide additional and more uniform electromagnetic energy dissipation, even when mechanical contact conditions vary. For sensor-oriented measurement environments, such stability is often more critical than achieving maximum attenuation, as consistent EMI suppression directly improves testing repeatability and reduces uncertainty.

Therefore, the absolute attenuation enhancement at the front side is limited, and the Fe_3O_4-based O-rings play a crucial role in stabilizing EMI shielding performance, reinforcing their suitability for reliable sensor testing in 5G-enabled EMI environments. Although the present results demonstrate that increasing the Fe_3O_4 loading improves the attenuation stability of the shielding enclosure, the corresponding intrinsic electromagnetic properties of the ferrite–epoxy composites, such as complex magnetic permeability and dielectric loss, were not characterized in this study. Such measurements would provide further insight into the relationship between material properties and RF attenuation behavior. This characterization will be included in future work to establish a more comprehensive correlation between the electromagnetic properties of the composites and the shielding performance of the proposed enclosure.

Figure 6 shows the attenuation variations measured at the right side of the pressing rod for different numbers of aluminum foil layers and hybrid configurations consisting of three aluminum foils stacked with a copper sheet under various applied pressures at selected frequencies. In the figure, "None" denotes the reference condition without aluminum foil or copper shielding layers. As shown in Figs. 6(a)–6(d), corresponding to the 1–5.5 GHz frequency range, most shielding configurations incorporating aluminum foils or the aluminum–copper hybrid structure exhibit a clear improvement in attenuation compared with the unshielded case. An exception is observed at 2.5 GHz, where the enhancement provided by a single-layer aluminum foil is relatively limited, indicating insufficient shielding effectiveness at this frequency. In contrast, configurations with an increased number of aluminum foil layers and the hybrid aluminum–copper structure demonstrate more pronounced attenuation enhancement, suggesting that multilayer metallic shielding is more effective in this frequency range. At higher frequencies of 6.5 and 7.5 GHz, the improvement in attenuation becomes less significant for all configurations. The reduced attenuation improvement observed above 6.5 GHz suggests that the microwave absorption characteristics of the present Fe_3O_4–epoxy composite gradually become less effective at higher frequencies. Although Fe_3O_4 was selected in this study because of its favorable balance between microwave absorption capability, fabrication simplicity, chemical stability, and cost-effectiveness, other microwave-absorbing materials such as MnZn ferrites and carbonyl iron exhibit different magnetic loss mechanisms and may provide improved attenuation performance in high-frequency bands.

A comparative investigation of these alternative absorbing materials will be conducted in future work to further enhance the broadband shielding effectiveness of the proposed enclosure. In this study, we emphasize the experimental verification of the proposed shielding enclosure. Future work will incorporate electromagnetic finite element simulations to visualize RF signal leakage paths, analyze high-frequency attenuation limitations, and correlate the simulated field distributions with the measured S-parameter results for further optimization of the enclosure design. This behavior may be attributed to the reduced skin depth and increased sensitivity to geometric discontinuities at higher frequencies, which limit the incremental shielding benefit of additional metallic layers. Regarding pressure effects, Fig. 6 indicates that applied pressure generally has a minor effect on attenuation, except at 2.5 GHz for the single-layer aluminum foil configuration, where pressure-dependent contact conditions appear to play a more notable role. Importantly, Fig. 6 also reveals that the use of multiple aluminum foil layers and aluminum–copper hybrid structures significantly reduces attenuation variability across repeated measurements. This reduced fluctuation indicates improved shielding stability, which is particularly advantageous for sensor-oriented measurement environments, where consistent EMI suppression is essential for ensuring reliable and repeatable sensor performance.

Figure 7 presents the attenuation variations measured at the front side of the pressing rod for different numbers of aluminum foil layers and hybrid configurations consisting of three aluminum foils stacked with a copper sheet under various applied pressures at selected frequencies. As shown in Figs. 7(d) and 7(e), corresponding to 5.5 and 6.5 GHz, the introduction of aluminum foils and copper sheets does not result in a significant enhancement in attenuation. This behavior is consistent with the observations in Fig. 6, where the incremental shielding

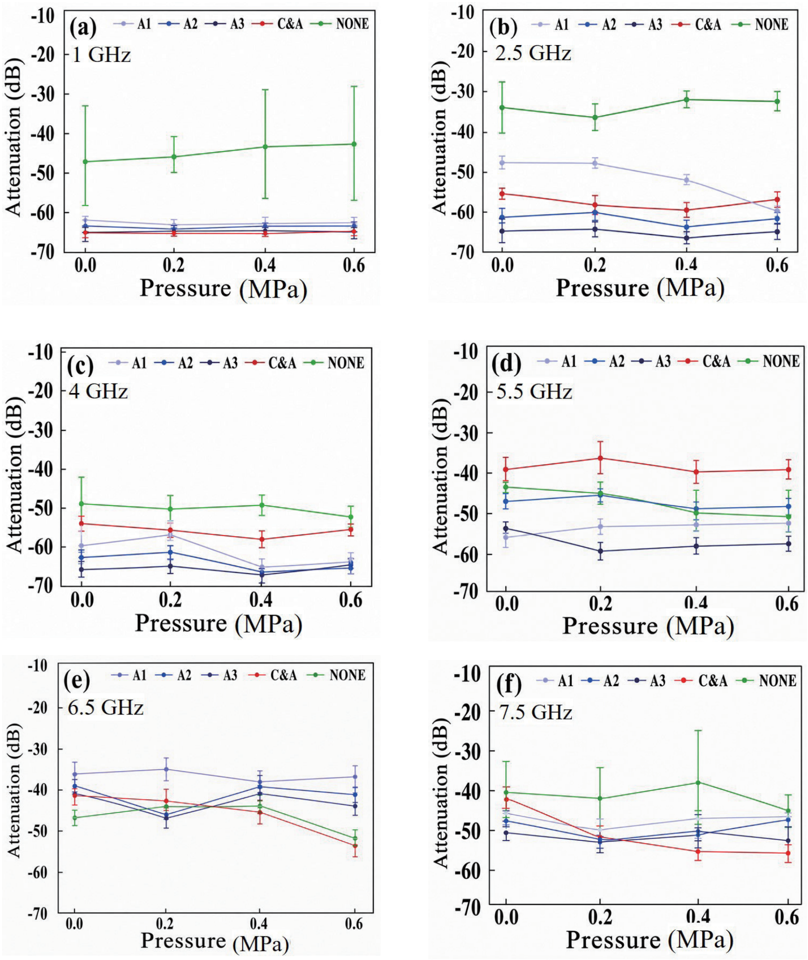

Fig. 6. (Color online) Attenuation variations measured at the right side of the pressing rod for different numbers of aluminum foil layers and hybrid configurations consisting of three aluminum foils stacked with a copper sheet under different applied pressures at various frequencies: (a) 1, (b) 2.5, (c) 4, (d) 5.5, (e) 6.5, and (f) 7.5 GHz.

improvement at higher frequencies becomes less pronounced. In contrast, at most other frequencies—specifically 1–4 GHz and 7.5 GHz, as illustrated in Figs. 7(a)–7(c) and Fig. 7(f)—the incorporation of aluminum foils and aluminum–copper hybrid structures leads to a clear and notable increase in attenuation compared with the unshielded case. These results indicate that metallic shielding layers are particularly effective in the low-to-mid frequency range, where reflection and absorption losses contribute more significantly to EMI suppression. The consistency between the front-side measurements (Fig. 7) and the right-side measurements (Fig. 6) further confirms the robustness of the multilayer and hybrid shielding strategy.

Regarding the effect of applied pressure, Fig. 7 shows that pressure effects are generally limited. A notable exception occurs at 4 GHz [Fig. 7(c)], where the attenuation of the unshielded configuration is more sensitive to applied pressure, likely due to pressure-dependent contact conditions at potential leakage paths. Once aluminum foils or hybrid metallic layers are introduced, the attenuation becomes largely insensitive to pressure variations. This pressure-independent behavior, also observed in Fig. 6, suggests that metallic shielding layers effectively

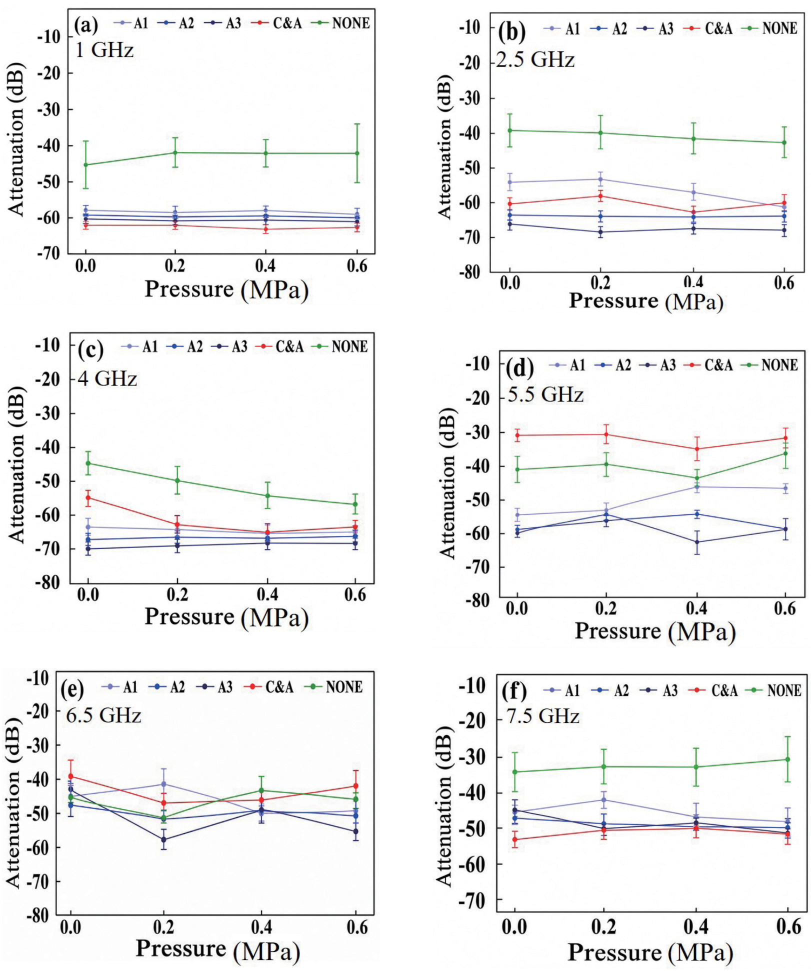

Fig. 7. (Color online) Attenuation variations measured at the front side of the pressing rod for different numbers of aluminum foil layers and hybrid configurations consisting of three aluminum foils stacked with a copper sheet under different applied pressures at various frequencies: (a) 1, (b) 2.5, (c) 4, (d) 5.5, (e) 6.5, and (f) 7.5 GHz.

dominate the EMI suppression mechanism. Overall, the combined results of Figs. 6 and 7 demonstrate that multilayer aluminum foils and aluminum–copper hybrid structures not only enhance attenuation but also improve RF signal attenuation stability across different measurement locations. Such stable and location-insensitive EMI shielding performance is particularly advantageous for sensor testing environments, where repeatable EMI suppression is essential for ensuring reliable and reproducible measurements under practical operating conditions.

4. Conclusions

In this study, we systematically evaluated the electromagnetic EMI shielding performance of an automated cylindrical enclosure integrating ferrite-filled O-rings and multilayer metallic shielding structures for sensor-oriented 5G IoT applications. RF signal attenuation measurements at multiple locations around the pressing rod confirm that both material composition and structural configuration strongly affect shielding effectiveness and testing stability. For the ferrite-based O-rings, the incorporation of Fe_3O_4 powder markedly improves RF signal attenuation stability across the investigated frequency range. Although the enhancement in peak attenuation depends on frequency and applied pressure, O-rings containing Fe_3O_4, particularly at higher weight fractions, consistently exhibit smaller attenuation fluctuations than O-rings without magnetic fillers. This improvement is attributed to magnetic loss mechanisms that provide more uniform electromagnetic energy dissipation under varying mechanical contact conditions. Such stability is especially valuable in sensor testing environments, where repeatability and low uncertainty are critical. Metallic shielding layers further enhance EMI suppression. Multilayer aluminum foils and aluminum–copper hybrid structures demonstrate a clear attenuation improvement in the low-to-mid frequency range (1–5.5 GHz) and effectively reduce attenuation variability across repeated measurements. Although the incremental benefit decreases at higher frequencies, these metallic configurations dominate the shielding behavior and significantly reduce pressure-dependent effects at potential leakage paths. Overall, the combined use of ferrite-filled O-rings and multilayer metallic shielding structures provides a robust and stable EMI-controlled environment. The proposed design provides a stable electromagnetic testing environment with the potential to support reliable sensor characterization, automated RF testing, and quality control in 5G-enabled IoT systems. Future work will validate these applications using practical sensor devices operating under realistic testing conditions.

Acknowledgments

This work was supported by Summit-Tech Resource Corp. and by projects under Nos. NSTC 113-2221-E-390-011 and NSTC 114-2622-E-390-001.

References

1 A.I. Zreikat, Z. AlArnaout, A. Abadleh, E. Elbasi, and N. Mostafa: Computers **14** (2025) 250.
2 https://appinventiv.com/blog/5g-iot-technology/ (accessed Sep. 2025).
3 S. Saini, P. Kumar, P. Gupta, R. Kant, M. K. Khanna, P. Jhajharia, B. K. Kuanr, and V. Kumar: J. Alloys Compd. **1022** (2025) 179969.
4 D. Foo Kune, J. Backes, S. S. Clark, D. Kramer, M. Reynolds, and K. Fu: 2013 IEEE Symp. Security and Privacy (Berkeley, CA, USA) (2013) 145–159.
5 S. Dutta: J. Emerg. Technol. Innov. Res. **12** (2025) e305.
6 J. H. Kwon, C. H. Hyoung, and H. H. Park: Electronics **13** (2024) 4345.
7 M. S. Hareesh, J. Praveen, and G. Sumesh: Nanoscale Adv. **7** (2025) 4510.
8 J. T. Orasugh and S. S. Ray: ACS Omega **8** (2023) 8134.
9 X. Xiang, Z. Yang, G. Fang, Y. Tang, Y. Li, Y. Zhang, D.-H. Kim, and C. Liu: Mater. Today Phys. **36** (2023) 101184.
10 S. S. Sefati and S. Halunga: Trans. Emerg. Telecommun. Technol. **34** (2023) e4770.
11 A. I. Zreikat, Z. AlArnaout, A. Abadleh, E. Elbasi, and N. Mostafa: Computers **14** (2025) 250.
12 Y.-F. Wang, L. Zhu, L. Han, X.-H. Zhou, X. Li, and G. Ji: ACS Appl. Nano Mater. **6** (2023) 9491.
13 S. Bao, Y. Wang, H. Lv, X. Li, and G. Ji: Nano Res. **17** (2024) 1.